

# KLDrive: Fine-Grained 3D Scene Reasoning for Autonomous Driving based on Knowledge Graph

Ye Tian<sup>1</sup>, Jingyi Zhang<sup>1</sup>, Zihao Wang<sup>1</sup>, Xiaoyuan Ren<sup>1</sup>,  
Xiaofan Yu<sup>2</sup>, Onat Gungor<sup>1</sup>, Tajana Rosing<sup>1</sup>

<sup>1</sup>University of California San Diego, La Jolla, California, USA

<sup>2</sup>University of California Merced, Merced, California, USA

{yet002,jiz290,ziw140,x6ren,ogungor,tajana}@ucsd.edu,xiaofanyu@ucmerced.edu

## Abstract

Autonomous driving requires reliable reasoning over fine-grained 3D scene facts. Fine-grained question answering over multi-modal driving observations provides a natural way to evaluate this capability, yet existing perception pipelines and driving-oriented large language model (LLM) methods still suffer from unreliable scene facts, hallucinations, opaque reasoning, and heavy reliance on task-specific training. We present KLDrive, the first knowledge-graph-augmented LLM reasoning framework for fine-grained question answering in autonomous driving. KLDrive addresses this problem through designing two tightly coupled components: an energy-based scene fact construction module that consolidates multi-source evidence into a reliable scene knowledge graph, and an LLM agent that performs fact-grounded reasoning over a constrained action space under explicit structural constraints. By combining structured prompting with few-shot in-context exemplars, the framework adapts to diverse reasoning tasks without heavy task-specific fine-tuning. Experiments on two large-scale autonomous-driving QA benchmarks show that KLDrive outperforms prior state-of-the-art methods, achieving the best overall accuracy of 65.04% on NuScenes-QA and the best SPICE score of 42.45 on GVQA. On counting, the most challenging factual reasoning task, it improves over the strongest baseline by 46.01 percentage points, demonstrating substantially reduced hallucinations and the benefit of coupling reliable scene fact construction with explicit reasoning.

## Keywords

Autonomous Driving, Knowledge Graph, Large Language Model, Scene Reasoning

## 1 Introduction

Autonomous driving relies on accurate understanding of fine-grained scene facts, including object identities, motion states, and spatial relations [27, 46]. These facts directly govern high-level decisions [35], such as braking, acceleration, lane changes, and turning maneuvers. Reliable reasoning over the

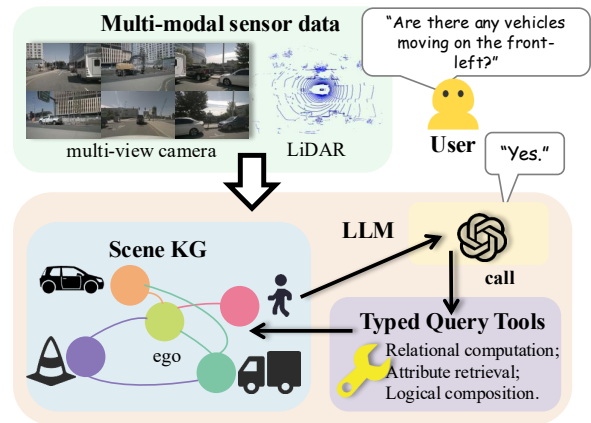


**Figure 1: KLDrive: fact-based scene question answering via a 3D scene KG and a tool-constrained LLM agent.**

3D driving scene therefore forms a critical interface between perception and planning.

Fine-grained question answering (QA) over driving scenes provides a natural and effective testbed for evaluating whether a system can understand fine-grained scene facts [22, 25, 28, 38]. Given a temporal window of multi-modal sensor observations, primarily multi-view cameras and LiDAR, together with a factual query about the current scene, the system is expected to understand and answer questions about object existence, motion states, counts, and spatial relations. For example, it may need to count how many vehicles are approaching the ego vehicle within a specified distance range, or determine whether there exists a moving target in a particular relative direction of the ego vehicle. Unlike conventional perception tasks that primarily evaluate recognition or localization accuracy, fine-grained QA instead tests whether the system can recover and reason over the structured scene facts that truly matter for driving. Therefore, it exposes weaknesses along the perception-to-reasoning pipeline, thereby offering more targeted evidence for model diagnosis, system improvement, and reliability assessment in safety-critical scenarios.

In this context, we focus on an important problem that remains insufficiently addressed: given multi-modal temporal sensor data, how can a system understand a complex

driving scene and perform reliable reasoning? Notably, we study such fine-grained complex reasoning in an offline analysis setting. At the current stage, we primarily focus on the accuracy of the reasoning results and the reliability of the reasoning process, rather than millisecond-level online response speed. Once these more fundamental issues are better addressed, efficiency optimization for real-time deployment can be pursued as an important direction for future work.

Achieving this goal presents three key challenges. **(1) Reliable scene fact construction.** Fine-grained question answering relies on accurate object identities, motion states, and spatial relations. However, recovering such scene facts from multi-view camera and LiDAR streams is difficult due to illumination variations, occlusion, ego motion, and sensor noise. Even state-of-the-art detectors still produce missed detections, false positives, duplicate candidates, and inconsistent hypotheses, making their outputs unreliable as a direct basis for reasoning. **(2) Fact-grounded interpretable reasoning.** Autonomous driving is a safety-critical domain, which requires system answers to be supported by concrete and verifiable scene facts. However, existing end-to-end methods directly map inputs to answers in a black-box manner, resulting in opaque decision processes and hallucinations. Their outputs also cannot be traced back to specific and verifiable scene evidence. **(3) Task adaptation under limited supervision.** Fine-grained scene question answering spans diverse query forms and reasoning patterns, yet collecting large-scale annotated question-program pairs and conducting task-specific training for each deployment setting is costly and difficult to scale. Therefore, the system must efficiently adapt to diverse reasoning tasks under limited supervision, without relying on heavy task-specific fine-tuning pipelines.

Existing approaches still fall short of addressing the above challenges. As shown in Table 1, no representative method simultaneously provides strong perception ability, reasoning ability, freedom from task-specific training, and explainable reasoning. First, perception-based methods, such as RayDN [15], FocalFormer3D [4], and IS-Fusion [41], possess strong scene perception ability, but still lack the explicit reasoning capability required for fine-grained factual question answering. Second, large language models (LLMs) have demonstrated strong capability on general reasoning tasks [24, 32, 37], but remain prone to hallucinations in fine-grained spatial and factual reasoning [11, 18, 34]. To improve adaptation to autonomous driving scenarios, recent works have proposed driving-oriented LLM frameworks, such as DriveLM [28], LiDAR-LLM [39], MAPLM [2], and CREMA [43], by introducing task-specific encoders and training on large-scale driving data, representing the current state-of-the-art (SOTA) among LLM-based methods. However, as shown by our experiments, these methods still suffer

	Methods	Perception ability	Reasoning ability	No task-specific training	Explainable reasoning
Perception-based Methods	RayDN [15]	✓	✗	✗	✗
	FocalFormer3D [4]	✓	✗	✗	✗
	IS-Fusion [41]	✓	✗	✗	✗
Driving-oriented LLM frameworks	DriveLM [28]	✓	✓	✗	✗
	LiDAR-LLM [39]	✓	✓	✗	✗
	MAPLM [2]	✓	✓	✗	✗
	CREMA [43]	✓	✓	✗	✗
Ours	KLDrive	✓	✓	✓	✓

**Table 1: Comparison of existing representative methods and KLDrive. ✓ indicates the property is supported and ✗ indicates it is not.**

from severe hallucinations on fine-grained factual queries over 3D scenes. In addition, their reliance on task-specific training pipelines makes it difficult to efficiently adapt to diverse reasoning tasks under limited supervision. Moreover, these methods lack fact-grounded and interpretable reasoning, instead relying on end-to-end black-box mappings from multi-modal inputs to answers. Consequently, their predictions cannot be traced to concrete and verifiable facts, which is highly risky for safety-critical autonomous driving.

To bridge these gaps, we propose KLDrive, the first knowledge graph (KG)-augmented LLM reasoning framework for fine-grained question answering in autonomous driving. As shown in Figure 2, KLDrive designs two tightly coupled modules: reliable scene fact construction and an LLM agent for reasoning over scene facts. Specifically, **(1)** to recover reliable scene facts from noisy driving observations, KLDrive first formulates perception as a multi-source evidence construction problem. It consolidates complementary hypotheses from camera and LiDAR point clouds through cross-source pooling and temporal recovery, and proposes an energy model to resolve conflicts, refine a coherent and reliable set of scene entities, and organize them into the scene KG. **(2)** Built upon this scene KG, we design an LLM agent that plans over a constrained action space to perform fact-grounded and interpretable reasoning. Rather than directly generating answers, the LLM acts as a semantic planner that incrementally invokes tools and receives feedback under a Plan-Execute-Observe loop. Each action is executed on concrete scene entities, thereby turning the reasoning into an explicit and auditable process grounded in scene facts. **(3)** In addition, to support task adaptation under limited supervision, KLDrive avoids task-specific program supervision and heavy fine-tuning pipelines. Through the design of a constrained action space together with few-shot in-context exemplars, it guides the LLM to invoke different tools under explicit rules and constraints, thereby adapting to diverse reasoning tasks.

We implement KLDrive with Qwen3-7B as the LLM backbone without task-specific fine-tuning and conduct systematic evaluations on two large-scale fine-grained autonomous driving QA benchmarks, NuScenes-QA [25] and GVQA [28]. Extensive experiments show that KLDrive achieves the best

performance on both benchmarks. On the structured QA task of NuScenes-QA [25], KLDrive attains the best overall accuracy of 65.04%, surpassing the strongest baseline at 60.17%; on GVQA [28], it achieves the best SPICE score of 42.45. When the perceptual facts are fully correct, its overall accuracy further reaches 84.49%. More importantly, on counting, the most challenging fine-grained factual reasoning task, KLDrive achieves an accuracy of 64.46%, improving over the strongest baseline by 46.01 points, demonstrating a significant advantage in mitigating hallucinations of end-to-end methods.

## 2 How to Construct Reliable Scene KG?

### 2.1 Challenges

Fine-grained reasoning in 3D autonomous driving scenes requires more than recognizing isolated objects. It relies on a reliable scene representation that faithfully captures object identities, attributes, motion states, and spatial relations, as these structured scene facts form the basis of reasoning. Consequently, accurate perception and high-quality scene knowledge graph construction are prerequisites for reliable fine-grained scene understanding. However, building such a knowledge graph from real-world driving sensor streams remains highly challenging.

**Challenge 1: Imperfect Evidence Acquisition.** Real-world driving scenes are affected by occlusion, illumination variation, sensor noise, and modality-specific degradation, making it difficult for any single sensing pathway to produce uniformly reliable scene facts. Cameras provide rich semantic textures and visual cues that are critical for object recognition, but they are sensitive to lighting conditions. LiDAR provides accurate 3D geometry and depth measurements and is relatively robust to illumination changes, but it suffers from long-range sparsity and degraded reliability for distant objects. Fusion-based detectors often provide a better balance between semantic and geometric cues, yet their outputs are corrupted by cross-modal misalignment, synchronization noise, or fusion bias. As a result, directly constructing a scene graph from the hard decisions of a single detector is fragile. A more robust strategy is to treat perception as a multi-source evidence acquisition problem and aggregate complementary hypotheses from heterogeneous detectors into a unified candidate space.

**Challenge 2: Structured Ambiguity.** Even after aggregating multi-source evidence, the resulting candidate space still contains structured fuzziness rather than just independent noise. Some candidates correspond to redundant hypotheses of the same physical object across detectors, some are weakly observed in the current frame but supported by neighboring frames, and some may appear locally plausible in isolation while remaining incompatible with the global

scene interpretation. Therefore, recovering the final scene entities cannot be reduced to simple score thresholding or independent per-candidate classification. Instead, it requires structured inference over the entire candidate set, where the selected entities should jointly satisfy strong evidence support, low redundancy, temporal consistency, and semantic plausibility.

### 2.2 EBM Background

Energy-based models (EBMs) [9, 36] provide a framework for structured prediction by associating a scalar energy with each input-output configuration, where lower energy indicates higher compatibility between the observed evidence and the predicted output. Given observed evidence  $\mathbf{x}$  and a structured output space  $\mathcal{Y}(\mathbf{x})$ , inference takes the form:

$$\mathbf{y}^* = \arg \min_{\mathbf{y} \in \mathcal{Y}(\mathbf{x})} E_\theta(\mathbf{y}, \mathbf{x}), \quad (1)$$

where  $E_\theta$  is a learnable energy function and  $\mathbf{y}^*$  denotes the lowest-energy output under the observed evidence. In this way, EBM does not make isolated local decisions for individual hypotheses, but evaluates the compatibility of a structured output as a whole.

This mechanism is particularly suitable for our problem. In scene entity recovery, the goal is not to decide whether each candidate should be retained independently, but to infer a subset of scene entities that is jointly well supported by the available evidence and coherent at the scene level. The final decision should account for multiple heterogeneous factors, including detector confidence, cross-source corroboration, pairwise redundancy, temporal support, and attribute-level consistency. EBMs provide a principled way to integrate these factors into a unified refinement objective, so that the final output is determined by the overall quality of the recovered scene interpretation.

However, applying EBM refinement to driving scenes is nontrivial. The energy function must reconcile heterogeneous detector outputs, distinguish harmful redundancy from useful temporal corroboration, and encode semantic and physical consistency while remaining tractable for inference over a large combinatorial output space. These requirements make the refinement stage both essential and challenging. To address these challenges, we design an energy-based evidence refinement framework that jointly evaluates support, interaction, temporal consistency, and semantic plausibility over pooled multi-source and multi-frame candidates, and recovers a refined set of reliable scene entities for subsequent scene KG construction.

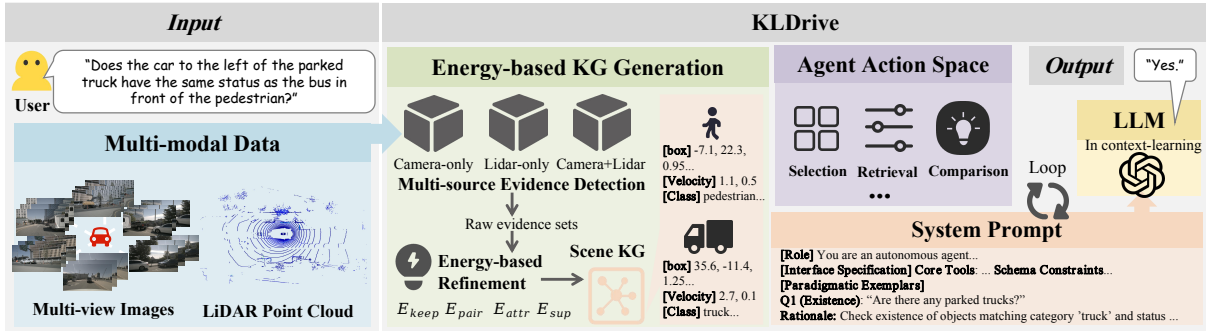


Figure 2: Overview of KLDrive, which converts multi-modal sensor data and a natural-language query into a scene KG, applies generic reasoning tools, and uses an in-context-learned LLM agent to produce a fact-grounded answer.

### 3 KLDrive Overview

KLDrive is built on a crucial design principle: complex and fine-grained scene question answering requires both a trustworthy scene representation and a reliable reasoning process. To this end, as illustrated in Figure 2, the system is organized into two tightly coupled stages. The first stage converts noisy multi-modal driving observations into a reliable scene KG by consolidating complementary multi-source evidence, refining candidate scene entities with an energy-based model, and organizing the refined entities into structured scene facts. The second stage performs question answering over this KG using an LLM agent that plans and executes grounded symbolic operations under a bounded action space. By coupling energy-based scene KG generation with LLM-driven orchestration and reasoning, KLDrive produces accurate, interpretable answers for complex 3D driving scenes.

## 4 Energy-based Knowledge Graph Generation

### 4.1 Multi-source Evidence Detection.

To build reliable scene facts, KLDrive first acquires object evidence from synchronized multi-view images and LiDAR point clouds. Since real-world driving scenes are affected by occlusion, illumination variation, sensor noise, and modality-specific degradation, no single sensing pathway can provide uniformly reliable evidence. As illustrated in Figure 2, we therefore formulate perception as a multi-source evidence acquisition problem and collect complementary hypotheses from camera-based, LiDAR-based, and fusion detectors. In our implementation, the detector set is instantiated with RayDN [15], FocalFormer3D [4], and IS-Fusion [41], selected for their strong empirical performance and complementary sensing characteristics. They together provide semantically rich visual evidence, geometrically grounded LiDAR evidence, and cross-modal corroborative evidence.

Formally, let  $\mathcal{M}$  denote the detector set. For frame  $\tau$ , each detector  $m \in \mathcal{M}$  processes its corresponding modality subset

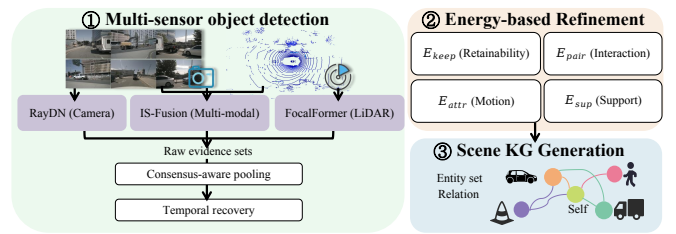


Figure 3: Energy-based scene KG generation model.

and produces a raw evidence set

$$\mathcal{Y}_\tau^m = \left\{ \left( \mathbf{b}_i^{\tau,m}, c_i^{\tau,m}, s_i^{\tau,m} \right) \right\}_{i=1}^{M_{\tau,m}},$$

where  $\mathbf{b}_i^{\tau,m}$  denotes the object state,  $c_i^{\tau,m}$  the semantic class label, and  $s_i^{\tau,m} \in [0, 1]$  the detector confidence. The union of all  $\mathcal{Y}_\tau^m$  forms a heterogeneous raw evidence space, which is then consolidated into a unified candidate space by the consensus-aware pooling stage.

### 4.2 Evidence Pooling and Recovery

Although the detectors provide complementary evidence, their outputs remain heterogeneous in geometric bias and confidence scale, and thus cannot yet form a unified evidence space. Moreover, real objects may still be weakly supported or entirely missing in the current frame due to occlusion, motion blur, or temporary sensing degradation. We therefore combine consensus-aware cross-source pooling with temporal recovery over neighboring frames to form a unified evidence space with explicit temporal support for the subsequent energy-based refinement stage.

**Evidence Pooling.** We first perform consensus-aware pooling over same-frame detector outputs. All raw evidence items are transformed into a shared ego-centric coordinate frame, and detector-specific confidence scores are normalized to reduce cross-source scale mismatch. We then associate hypotheses from different detectors when they share the same semantic label and remain geometrically consistent in BEV position, size, and heading. Each associated group is

aggregated into one pooled candidate  $\tilde{y}_i^\tau$ , whose 3D state, semantic label, and confidence score are obtained by aggregating its supporting evidence items. Importantly, the supporting detector identities are explicitly retained in a provenance set  $\mathcal{M}_i^\tau \subseteq \mathcal{M}$ , allowing the subsequent refinement stage to determine which detectors support each candidate and how strong that cross-source corroboration is.

**Temporal Recovery.** While cross-source pooling improves evidence consistency within the current frame, the resulting candidate space may still miss real objects that are only weakly observed or temporarily absent due to short-term occlusion, motion blur, or transient sensing degradation. To address this limitation, we further incorporate evidence from neighboring frames around  $\tau$  and recover missing object states through short-horizon temporal association and interpolation. Specifically, we associate pooled candidates across a short temporal window to form tracklets in the global frame, and perform trajectory-based completion over valid gaps between two observed states. For a tracklet with observed centers  $\mathbf{p}_i^{\tau^-}$  and  $\mathbf{p}_i^{\tau^+}$  at two neighboring frames, the missing center at an intermediate frame  $\tau$  is recovered by linear interpolation:

$$\tilde{\mathbf{p}}_i^\tau = (1 - \alpha)\mathbf{p}_i^{\tau^-} + \alpha\mathbf{p}_i^{\tau^+}, \quad \alpha = \frac{\tau - \tau^-}{\tau^+ - \tau^-} \in [0, 1]. \quad (2)$$

The recovered center is then projected back to the local sensor frame at time  $\tau$ , while box attributes and semantic labels are inherited from the nearest observed state along the tracklet. Each recovered hypothesis is assigned the average confidence of its two neighboring observations and merged into the candidate pool.

**Evidence Space.** After cross-source pooling and temporal recovery, we obtain the final pooled candidate set  $\tilde{\mathcal{Y}}_\tau = \{\tilde{y}_i^\tau\}_{i=1}^{K_\tau}$ , where each candidate  $\tilde{y}_i^\tau$  includes its aggregated 3D state, semantic label, pooled confidence  $\tilde{s}_i^\tau$ , provenance set  $\mathcal{M}_i^\tau$ , and an evidence-type indicator  $g_i$  that distinguishes directly observed candidates from temporally recovered ones. This pooled candidate set serves as the input to the subsequent energy-based refinement stage.

### 4.3 Energy Model Formulation.

Given the pooled candidate set, KLDive aims to recover the final scene entities at frame  $\tau$ . This is challenging because the desired output cannot be obtained by evaluating each candidate independently: whether a candidate should be retained depends not only on its own evidence, but also on cross-source corroboration, interactions with other candidates, and the global coherence of the resulting scene interpretation.

Inspired by energy-based modeling, we formulate this process as a structured subset refinement problem over  $\tilde{\mathcal{Y}}_\tau$  and design a refinement energy model to favor candidate subsets that recover reliable scene entities, thereby enabling

higher-quality scene KG construction. Let  $\mathbf{z}_\tau = \{z_i^\tau\}_{i=1}^{K_\tau}$  denote binary selection variables, where  $z_i^\tau = 1$  indicates that candidate  $\tilde{y}_i^\tau$  is retained in the final scene entity set, and  $z_i^\tau = 0$  otherwise. We define the total refinement energy as

$$E(\tilde{\mathcal{Y}}_\tau, \mathbf{z}_\tau) = \sum_i z_i^\tau E_{\text{keep}}(i) + \sum_{i < j} z_i^\tau z_j^\tau E_{\text{pair}}(i, j) + \sum_i z_i^\tau E_{\text{attr}}(i) + \sum_i z_i^\tau E_{\text{sup}}(i), \quad (3)$$

where  $E_{\text{keep}}$  captures the unary retainability of each candidate,  $E_{\text{pair}}$  models pairwise interactions among candidates,  $E_{\text{attr}}$  enforces motion-state plausibility, and  $E_{\text{sup}}$  penalizes insufficient temporal or contextual support. The refinement objective is to optimize  $\mathbf{z}_\tau$  such that the selected candidate subset attains low total energy under Eq. (3). Lower energy corresponds to a scene entity set with stronger evidence support, less redundancy, and better semantic and temporal consistency.

**Retainability and Interaction Modeling.** We first model candidate-level evidence strength through the keep component, which determines whether an individual candidate is sufficiently supported to be retained. Specifically, we define

$$E_{\text{keep}}(i) = -\ell_i^{\text{keep}}, \quad \ell_i^{\text{keep}} = a_{g_i} \tilde{s}_i^\tau + b_{g_i} + \alpha_{\text{src}} k_i, \quad (4)$$

where  $\tilde{s}_i^\tau$  is the pooled confidence score of candidate  $\tilde{y}_i^\tau$ , and  $g_i$  denotes its evidence type, indicating whether the candidate is directly observed or temporally recovered. The parameters  $a_{g_i}$  and  $b_{g_i}$  calibrate the pooled confidence according to the candidate’s evidence type. Moreover,  $k_i = |\mathcal{M}_i^\tau|/|\mathcal{M}|$  denotes the normalized cross-source corroboration strength derived from the provenance set  $\mathcal{M}_i^\tau \subseteq \mathcal{M}$ . Therefore,  $E_{\text{keep}}$  favors candidates that have both stronger calibrated confidence and stronger cross-source support.

We next model pairwise interactions among candidates through the pair component:

$$E_{\text{pair}}(i, j) = \lambda_{\text{dup}} r_{ij}^{\text{dup}} - \lambda_{\text{tmp}} r_{ij}^{\text{tmp}}, \quad (5)$$

where  $r_{ij}^{\text{dup}}$  measures the degree to which candidates  $\tilde{y}_i^\tau$  and  $\tilde{y}_j^\tau$  provide redundant explanations of the same physical object, using pairwise cues such as BEV distance, overlap, and semantic label consistency. In contrast,  $r_{ij}^{\text{tmp}}$  measures pairwise consistency induced by temporally supported evidence, favoring candidate pairs whose geometry and semantics remain compatible with neighboring-frame corroboration. Accordingly,  $E_{\text{pair}}$  penalizes redundant candidate pairs while preserving pairwise consistency supported by neighboring-frame corroboration.

**Semantic and Support-guided Correction.** Beyond unary evidence strength and pairwise interaction, we further regularize candidate selection through motion-state plausibility and support sufficiency. Specifically, the attr component

is defined as

$$E_{\text{attr}}(i) = -\log p(a_i | v_i), \quad (6)$$

where  $a_i$  denotes the motion state of candidate  $\hat{y}_i^\tau$ , and  $v_i$  denotes its kinematic evidence derived from the estimated speed magnitude together with its local motion context. Thus,  $E_{\text{attr}}$  assigns lower energy to candidates whose motion states are more consistent with their kinematic evidence, enforcing an additional physical plausibility constraint beyond geometric support alone. We further model support sufficiency through the sup component:  $E_{\text{sup}}(i) = \beta_{\text{tmp}} [m_{\text{tmp}} - u_i]_+ + \beta_{\text{ctx}} [m_{\text{ctx}} - d_i]_+$ , where  $u_i$  denotes the aggregated temporal support of candidate  $i$  from neighboring-frame evidence,  $d_i$  denotes the local evidence density around the candidate,  $m_{\text{tmp}}$  and  $m_{\text{ctx}}$  are the corresponding minimum support thresholds, and  $[x]_+ = \max(x, 0)$ . Accordingly,  $E_{\text{sup}}$  assigns higher energy to candidates whose temporal corroboration from neighboring frames or local evidence density remains insufficient, thereby suppressing weakly grounded hypotheses.

Together, the four terms define a structured refinement objective over the pooled candidate set. In our implementation, the learnable parameters are estimated using binary supervision on pooled candidates, and inference optimizes Eq. (3) over  $\mathbf{z}_\tau$  to produce the refined entity set  $\hat{\mathcal{Y}}_\tau$  for subsequent scene KG construction.

#### 4.4 Scene Knowledge Graph Generation

Given the refined entity set  $\hat{\mathcal{Y}}_\tau$  obtained after energy-based refinement, we next construct a scene knowledge graph for structured LLM reasoning. At frame  $\tau$ , each refined entity is instantiated as a node  $v_i \in \mathcal{V}_\tau$  with attribute vector  $\mathbf{a}_i^\tau$ , which encodes its geometry, motion state, semantic label, and confidence. In this way, the refined candidate subset is converted into an object-centric symbolic scene representation.

Rather than explicitly materializing all pairwise edges, we represent inter-object relations through a compact library of relational operators  $\Psi$  defined over node attributes. For any pair of nodes  $(v_i, v_j)$  and operator  $\psi \in \Psi$ , the corresponding relation is computed as:  $\mathbf{r}_{ij, \psi}^\tau = \psi(\mathbf{a}_i^\tau, \mathbf{a}_j^\tau)$ . For example, a basic geometric operator produces the relative displacement and distance between two entities:

$$\mathbf{r}_{ij, \text{geo}}^\tau = [\Delta x_{ij}, \Delta y_{ij}, \Delta z_{ij}, \|\Delta \mathbf{p}_{ij}\|_2]^\top.$$

These operator-defined relations provide the basis for higher-level query-facing reasoning over spatial, semantic, and motion-aware scene structure. Since full pairwise relation materialization incurs  $O(|\mathcal{V}_\tau|^2)$ , KLDrive instantiates only the relations relevant to the queried objects and reasoning operators. This query-adaptive construction preserves the structured scene information needed for reasoning while avoiding

unnecessary calculation, supporting the subsequent LLM-driven orchestration and reasoning stage.

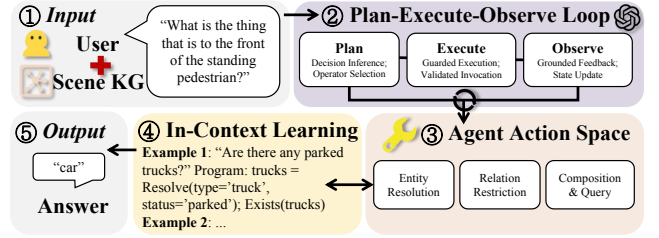


Figure 4: Proposed LLM Scene-Reasoning Agent.

## 5 LLM-Driven Orchestration and Reasoning

Built on the constructed scene KG, we design an LLM agent for reliable fine-grained scene reasoning. As illustrated in Figure 4, the agent operates over a bounded scene-query algebra defined on the scene KG, while the LLM serves as a semantic planner that selects executable operator calls to analyze complex queries step by step rather than directly generating answers. The overall process follows a *Plan-Execute-Observe* loop: the planner proposes an action, the executor applies it to the scene KG, and the grounded observation is fed back into subsequent planning. This design turns scene reasoning into an explicit and auditable reasoning process over structured scene facts.

### 5.1 The Plan-Execute-Observe Loop.

We design an LLM agent that realizes question answering step by step through a *Plan-Execute-Observe* loop. Given the query, the LLM planner first selects the next symbolic action from the bounded action space. The executor then applies this action to the scene KG and returns a grounded observation, which is written back into the interaction context to guide subsequent planning. This process repeats until the reasoning chain reaches a terminal answer. The loop naturally adapts to question complexity. For simple queries, a single grounded action may be sufficient to produce the answer. For compositional queries involving multiple entities, spatial relations, and status comparisons, the loop unfolds into a multi-step sequence that progressively resolves references, restricts candidate subsets, composes intermediate results, and issues typed queries over the grounded scene state. In this way, the full reasoning program is constructed online through successive grounded executions rather than produced as unconstrained text. Because each step must instantiate a valid operator and consume verified intermediate results, the resulting reasoning process forms an explicit symbolic trace over the scene KG. We next describe the agent action space underlying this iterative reasoning process.

### Structured Prompt for our Scene Reasoning Agent

- **[Role]** You are an agent that answers fine-grained questions about a 3D driving scene. You must decompose each question into executable operations over the scene, and you must not introduce entities or relations that are not supported by the operators.
- **[Scene-Query Algebra]** The scene is queried through a constrained set-based algebra.  $\text{Resolve}(\dots)$  returns the entity set satisfying the specified attribute predicates.  $\text{RelSelect}(\text{ref}, \text{rel}, \dots)$  returns the entities satisfying the specified predicates and relation  $\text{rel}$  with respect to reference object  $\text{ref}$ .  $\text{Intersect}(A, B)$  composes two entity sets.  $\text{Count}(V)$  and  $\text{Exists}(V)$  query the size and non-emptiness of an entity set.  $\text{GetType}(V)$  and  $\text{GetStatus}(V)$  return a canonical type or status label from  $V$ .  $\text{SameStatus}(A, B)$  returns yes iff the two entity sets contain a valid pair with the same status.
- **[Reasoning Rules]** All intermediate variables must be entity sets, except typed outputs from  $\text{Count}$ ,  $\text{Exists}$ ,  $\text{GetType}$ ,  $\text{GetStatus}$ , and  $\text{SameStatus}$ . Spatial relations follow the ego-centric vocabulary  $\mathcal{R}$ . Reference sets are reduced to their canonical representative, and single-object relational references use the nearest valid instance. Arguments and outputs must stay within the bounded scene schema, including categories  $\mathcal{C}$ , statuses  $\mathcal{S}$ , relations  $\mathcal{R}$ , binary answers, and integers.
- **[Exemplars]**
  - **Question:** "Does the car to the left of the stopped truck have the same status as the bus in front of the cyclist?"
  - **Action:** `truck = Resolve(type='truck', status='stopped');`  
`car = RelSelect(truck, 'left', type='car');`; `cyclist = Resolve(type='cyclist');`  
`bus = RelSelect(cyclist, 'front', type='bus');`; `SameStatus(car, bus)`
- **[New Task] Question:** {QUESTION}

Figure 5: Structured system prompt for the LLM planner.

## 5.2 LLM Agent Action Space

We define the agent action space as a bounded scene-query algebra over the scene KG. Its central design principle is that every intermediate state must remain grounded in entities supported by the refined scene representation, rather than latent objects introduced by the language model. Formally, let  $\mathcal{V}_\tau$  denote the entity nodes in the scene KG at frame  $\tau$ , and represent an intermediate reasoning state as an entity subset  $\mathcal{U} \subseteq \mathcal{V}_\tau$ . Each node in  $\mathcal{V}_\tau$  carries a category label in  $\mathcal{C}$  and a status label in  $\mathcal{S}$ . When a subsequent operation requires a unique reference object or attribute query, we map  $\mathcal{U}$  to a deterministic representative  $\text{rep}(\mathcal{U})$ , defined by the current canonical ordering of the subset.

**Entity Resolution.** The first primitive maps a linguistic object description into a grounded entity subset. Let  $\pi$  denote a Boolean predicate over node attributes, for example  $c_i = \text{car} \wedge s_i = \text{moving}$ . We define  $\text{Resolve}(\pi) = \{v_i \in \mathcal{V}_\tau \mid \pi(v_i)\}$ . Thus,  $\text{Resolve}$  converts a natural-language description into an executable grounded state over perceived scene entities.

**Relational Restriction.** To support spatially conditioned queries, we define an ego-centric relational selection operator. Let  $\mathbf{d}_{\text{ego}} \in \mathbb{R}^2$  denote the ego heading vector, and let  $\mathcal{R}$  be a finite directional vocabulary. Given a reference subset  $\mathcal{U}_{\text{ref}}$  and a candidate predicate  $\pi$ , we first obtain the anchor node  $v_{\text{ref}} = \text{rep}(\mathcal{U}_{\text{ref}})$  with ground-plane position  $\mathbf{p}_{\text{ref}}$ . For each candidate node  $v_j$  with position  $\mathbf{p}_j$ , we compute the signed ego-centric angle  $\theta_{\text{ref},j} = \angle_{\text{signed}}(\mathbf{p}_j - \mathbf{p}_{\text{ref}}, \mathbf{d}_{\text{ego}}) \in (-\pi, \pi]$ . We then quantize  $\theta_{\text{ref},j}$  into a directional relation  $r \in \mathcal{R}$  through a deterministic mapping  $\Phi_{\text{angle}} : (-\pi, \pi] \rightarrow \mathcal{R}$ . In practice,  $\mathcal{R} = \{\text{front}, \text{front\_left}, \text{back\_left}, \text{back}, \text{back\_right}, \text{front\_right}\}$ , which aligns language-level directional expressions with ego-centric geometry. Accordingly, we define

$$\mathcal{U}_r = \{v_j \in \mathcal{V}_\tau \mid \pi(v_j) \wedge \Phi_{\text{angle}}(\theta_{\text{ref},j}) = r\}.$$

$$\text{RelSelect}(\mathcal{U}_{\text{ref}}, r, \pi) = \text{Sort}_{d(\cdot, v_{\text{ref}})}(\mathcal{U}_r).$$

where the result is returned in nearest-first order. In this way,  $\text{RelSelect}$  grounds spatial language in executable geometry while providing a deterministic ordering for downstream reference selection.

**Set Composition and Typed Queries.** Compositional questions are expressed through set composition and typed queries over grounded subsets. We define the basic set-level operators as

$$\begin{aligned} \text{Intersect}(\mathcal{U}_A, \mathcal{U}_B) &= \mathcal{U}_A \cap \mathcal{U}_B, \\ \text{Count}(\mathcal{U}) &= |\mathcal{U}|, \\ \text{Exists}(\mathcal{U}) &\in \{\text{yes}, \text{no}\}, \end{aligned}$$

where  $\text{Exists}$  returns yes iff  $\mathcal{U} \neq \emptyset$ . We further define typed queries over selected subsets:

$$\begin{aligned} \text{GetType}(\mathcal{U}) &= c(\text{rep}(\mathcal{U})) \in \mathcal{C}, \\ \text{GetStatus}(\mathcal{U}) &= s(\text{rep}(\mathcal{U})) \in \mathcal{S}, \\ \text{SameStatus}(\mathcal{U}_A, \mathcal{U}_B) &\in \{\text{yes}, \text{no}\}, \end{aligned}$$

where  $c(\cdot)$  and  $s(\cdot)$  return the category and status label of the selected node, respectively, and  $\text{SameStatus}$  returns yes iff  $s(\text{rep}(\mathcal{U}_A)) = s(\text{rep}(\mathcal{U}_B))$ . Together,  $\text{Resolve}$ ,  $\text{RelSelect}$ , and the operators above form a compact and executable scene-query algebra for fine-grained reasoning over the scene KG. For example, the question "How many cars are in front of the standing pedestrian?" can be expressed as  $\text{Count}(\text{RelSelect}(\text{Resolve}(\pi_{\text{ped,stand}}), \text{front}, \pi_{\text{car}}))$ , where  $\pi_{\text{ped,stand}}$  selects standing pedestrians and  $\pi_{\text{car}}$  selects cars.

## 5.3 LLM Planner with In-Context Learning

Given a natural-language query  $q$ , KLDive uses the LLM planner to incrementally construct an executable action sequence  $\Pi(q) = (\text{op}_1, \text{op}_2, \dots, \text{op}_K)$  over the bounded action space defined above. Rather than generating the full

program in a single pass, the planner operates within the Plan–Execute–Observe loop, where each step is determined jointly by the user query, the structured prompt, and the grounded interaction context accumulated so far. In this way, the LLM is responsible for analyzing the query and selecting valid operator calls over grounded intermediate states. However, collecting large-scale supervised fine-tuning data for question-driven tool invocation is prohibitively expensive, as it requires substantial manual annotation. Therefore, instead of relying on task-specific fine-tuning, we adopt an in-context learning paradigm to induce planning behavior from a pretrained LLM.

Specifically, we construct a structured system prompt  $\mathcal{P}$ , shown in Figure 5. The prompt first assigns the model a planner role for fine-grained 3D scene question answering, and then explicitly specifies the scene-query algebra as its admissible action space, including the available operators and their semantics. It further encodes the execution rules required for valid reasoning, such as maintaining intermediate variables as grounded entity subsets, reducing reference sets to deterministic representatives when needed, interpreting spatial relations in the ego frame, and constraining all arguments and outputs to the bounded schema  $(C, S, \mathcal{R})$ . Finally, we provide in-context Question–Program exemplars that demonstrate how representative queries should be decomposed into executable operator sequences. As a result, the prompt enables grounded query-to-program planning under explicit structural and geometric constraints, thereby completing the KG-based reasoning for fine-grained scene question answering.

## 6 Experimental Setup

### 6.1 Datasets

We evaluate KLDive on two large-scale public benchmarks, namely NuScenes-QA [25] and GVQA [28]. These two datasets systematically evaluate the fine-grained scene understanding and factual reasoning capabilities of KLDive from two levels: structured short-answer and sentence level comprehensive QA. (1) *NuScenes-QA* [25] is currently the largest public benchmark for factual reasoning in driving scenes. We select 39,704 challenging fine-grained factual reasoning questions, covering five high-level categories: *existence*, *counting*, *object query*, *status query*, and *comparison*. These questions require short structured answers, including binary yes/no responses, integer counts, and categorical labels such as object identity and motion status. (2) *GVQA* [28] is a QA benchmark for driving understanding with a richer coverage of dimensions. Besides factual understanding, it also includes speed prediction and driving behavior QA. Therefore, we select 104,030 QA tasks oriented towards understanding basic facts. These questions involve compositional queries over object

identity, motion status, existence, and quantity, and their answers are given in sentence form.

### 6.2 Metrics

We use dataset-specific metrics to account for the different answer formats in the two benchmarks, and additionally report inference latency to measure efficiency. (1) **Exact Match Accuracy**. For NuScenes-QA, where answers are short structured outputs, we follow the standard evaluation protocol [25] and report strict exact-match accuracy. We present accuracy for each question category as well as the overall accuracy. (2) **Sentence-level QA Metrics**. For GVQA [28], where answers are primarily sentence-form factual responses. We therefore adopt GVQA recommended metrics, including SPICE, METEOR, and CIDEr. These are widely used metrics for sentence-level QA evaluation, providing semantic correctness metrics of different dimensions for the generation of factual answers. We report these metrics using their standard scales, where higher values indicate better performance. (3) **Reasoning Time (s)**. To evaluate reasoning efficiency, we measure the average per-question inference latency. This metric reflects the end-to-end time required to generate an answer for a given question.

### 6.3 Baselines

We compare KLDive with three representative groups of baselines: (1) Perception-based pipelines with learned QA heads, (2) Foundation VLMs under few-shot in-context learning, and (3) driving-specialized multimodal LLM/VLM frameworks. Methods marked with <sup>†</sup> require task-specific training or fine-tuning, whereas methods marked with <sup>‡</sup> keep the backbone frozen and use few-shot in-context learning only.

(1) **Perception-based baselines**. We consider three SOTA perception backbones: RayDN<sup>†</sup> [15], FocalFormer3D<sup>†</sup> [4], and IS-Fusion<sup>†</sup> [41], corresponding to camera-only, LiDAR-only, and camera–LiDAR fusion settings. We attach benchmark-specific QA heads to their perception outputs. For NuScenes-QA, which requires short structured answers, we follow the standard setting and pair each detector with the MCAN QA head [44], which is trained together with the QA task. For DriveLM, whose answers are sentence-form factual responses, we pair each detector with a BERT-based answer head to produce sentence-level outputs. These baselines therefore test how far detector outputs can support fine-grained reasoning and QA without explicit knowledge graph.

(2) **Foundation VLMs**. To assess the ability of foundation VLMs models to reason and understand fine-grained autonomous driving problems, we evaluated several representative VLMs, including LLaVA-v1.6-Mistral-7B<sup>‡</sup> [16], InternVL-3.5-8B<sup>‡</sup> [33], and Qwen3Vision-8B<sup>‡</sup> [30]. These models take rendered multi-view camera images and the

Models	NuScenes-QA [25]					GVQA [28]			
	Acc ↑ (Exist)	Acc ↑ (Count)	Acc ↑ (Object)	Acc ↑ (Status)	Acc ↑ (Comparison)	Overall Acc ↑	SPICE ↑	METEOR ↑	CIDEr ↑
FocalFormer3D <sup>†</sup> [4]	50.28	0.01	0.55	0.22	47.36	24.02	14.41	0.21	0.56
RayDN <sup>†</sup> [15]	44.13	0.04	1.48	0.28	44.38	21.46	11.58	0.20	0.46
IS-Fusion <sup>†</sup> [41]	52.70	0.04	0.42	0.67	44.87	24.86	11.20	0.19	0.44
LLaVA-v1.6-mistral-7 <sup>‡</sup>	48.64	6.83	1.48	5.09	52.80	26.17	43.75	0.11	0.38
Internvl-3.5-8b <sup>‡</sup>	49.86	11.16	35.74	22.29	38.72	34.28	32.66	0.13	0.34
Qwen3Vision-8B <sup>‡</sup>	64.16	10.30	27.66	26.11	39.63	39.53	36.44	0.22	0.50
DriveLM <sup>†</sup> [28]	77.29	16.92	53.67	50.64	67.41	56.42	42.16	0.42	3.53
LiDAR-LLM <sup>†</sup> [39]	76.41	15.84	50.63	48.00	69.11	55.08	41.09	0.42	3.35
MAPLM <sup>†</sup> [2]	79.29	18.45	60.67	58.38	70.55	60.17	37.12	0.36	3.09
CREMA <sup>†</sup> [43]	73.17	15.69	53.69	52.63	72.03	55.26	39.05	0.39	3.27
KLDrive-KG <sup>‡</sup> (Ours)	74.67	64.46	54.30	57.84	53.23	65.04	42.45	0.41	3.48
KLDrive-GT <sup>‡</sup> (Ours)	<b>88.55</b>	<b>78.92</b>	<b>80.11</b>	<b>85.72</b>	<b>82.01</b>	<b>84.49</b>	<b>43.89</b>	<b>0.43</b>	<b>3.88</b>

**Table 2: Comparison for KLDrive with baselines on NuScenes-QA [25] and GVQA [28]. Bold numbers indicate the best performance. Methods marked with <sup>†</sup> trained since they have task-specific parameters, whereas methods marked with <sup>‡</sup> use frozen LLM with few-shot ICL only.**

question as input, and directly generate answers in an end-to-end manner. All model parameters are kept frozen, and adaptation is performed purely through few-shot in-context exemplars.

**(3) Driving-specialized LLM frameworks.** We further benchmark against representative recent SOTA baselines for multi-modal driving-scene understanding, including DriveLM<sup>†</sup> [28], LiDAR-LLM<sup>†</sup> [39], the official MAP- LM<sup>†</sup> [2], and CREMA<sup>†</sup> [43]. These methods build on foundation LLM backbones and introduce task-specific encoders, projectors, or adapters to better model driving-scene inputs and QA tasks. They represent strong recent baselines for LLM-based scene understanding in autonomous driving and closely related multimodal reasoning settings. We follow their official implementations and fine-tune them on both NuScenes-QA [25] and GVQA [28] dataset.

**(4) KLDrive variants.** We report two variants of our framework. KLDrive-KG is the full system, which constructs the scene KG from predicted perception outputs. KLDrive-GT is a variant that builds the KG directly from ground-truth annotations, in order to isolate reasoning performance from perception errors. Both variants use the same bounded query tool set and the same frozen LLM agent, controlled purely through few-shot in-context learning.

## 6.4 Implementation Details

For both NuScenes-QA [25] and GVQA [28] dataset, we randomly split the data into training and test sets with an 8:2 ratio. We implement KLDrive using PyTorch and Hugging-Face. For KLDrive, the perception front-end is trained on training dataset, while the reasoning agent uses a frozen Qwen3-7B backbone and is controlled solely through few-shot in-context learning, with no gradient updates. Experiments are conducted on a workstation equipped with an AMD Ryzen Threadripper 9985WX CPU, 768 GB RAM, and NVIDIA RTX A6000 GPUs. For edge-side latency evaluation, we use an NVIDIA Jetson Orin NX with 16 GB RAM.

## 7 Experimental Results

### 7.1 Overall Results

Table 2 summarizes the overall performance of all methods on NuScenes-QA [25] and GVQA [28] dataset. Across both benchmarks, the three baseline families exhibit a clear results: perception-based methods perform worst, and general foundation VLMs are improved, while driving-specialized LLM frameworks provide the strongest competing results after task-specific fine-tuning. Compared with these baselines, KLDrive further improves fine-grained scene understanding and reasoning. On NuScenes-QA, KLDrive-KG achieves the best overall accuracy of 65.04%, outperforming the strongest baseline, MAPLM, by 4.87 points. When the perceived result is completely accurate, the reasoning performance further increases to 84.49% with KLDrive-GT. On GVQA, KLDrive-KG also remains highly competitive against the strongest task-specific fine-tuned driving-oriented LLM/ MVLM frameworks, achieving the best SPICE score of 42.45 while maintaining comparable METEOR and CIDEr. Moreover, KLDrive-GT attains the best performance on all three metrics, reaching 43.89 SPICE, 0.43 METEOR, and 3.88 CIDEr.

Beyond the numerical gains, these results highlight the key advantage of the new paradigm introduced by KLDrive: it enables fact-grounded, transparent, and traceable QA reasoning. Unlike prior end-to-end methods, which map sensor inputs directly to answers through opaque trained representations, KLDrive first aggregates multi-sensor evidence from the scene and constructs a scene knowledge graph, and then uses the LLM as a planner to invoke tools step by step within a designed action space. Because the action space consists of deterministic operations over the scene KG, every answer is grounded in detected scene facts rather than produced by a potentially correct but unverified guess. The entire reasoning process is transparent, auditable, and traceable. Through explicit tool calls in the action space and the intermediate results they return, each answer can be traced step by step to concrete objects, attributes, and relations in the evidence

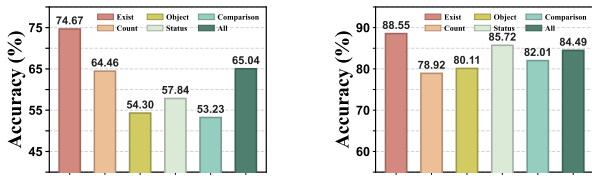


Figure 6: Comparison of KLDrive-KG (left) and KLDrive-GT (right) accuracy on different categories.

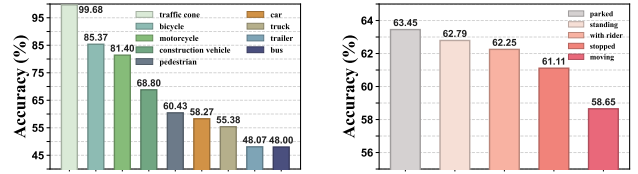


Figure 7: Comparison of KLDrive-KG accuracy across object categories (left) and attributes (right).

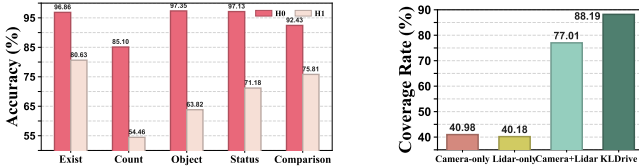


Figure 8: KLDrive-GT Accuracy for reasoning difficulty.

Figure 9: Coverage of each evidence space.

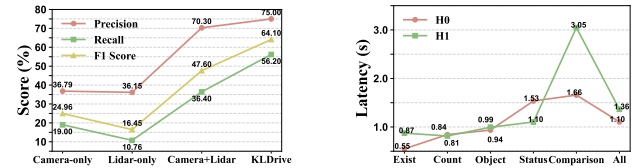


Figure 10: Effect of EBM-based refinement model.

Figure 11: Latency by QA category and difficulty.

space. As a result, the agent will not produce speculative answers that are not supported by detected evidence.

This advantage is especially evident on *counting* tasks, where KLDrive-KG reaches 64.46% accuracy, while the best baseline achieves only 18.45%, yielding a large gain of 46.01 points. However, the LLM-related baselines achieve an average accuracy of only 13.60%, suggesting serious hallucination issues. Compared with conventional perception-driven pipelines, KLDrive delivers significant gains across all tasks. Notably, these perception methods also serve as the detection backbones of KLDrive, therefore further highlights the necessity of our reasoning module design. Although such perception-driven methods can detect scene objects, they do not explicitly organize these detections into a structured scene knowledge graph or perform effective understanding over them. Overall, by transforming detected evidence into an executable scene KG and coupling it with a tool-driven reasoning agent, KLDrive effectively bridges perception and reasoning, achieving the best overall performance compared with the latest baselines.

## 7.2 Analysis of Reasoning Tasks

We further analyze performance across QA categories and reasoning difficulty levels to better understand the performance of KLDrive.

**QA Categories.** Figure 6 shows that both KLDrive-KG and KLDrive-GT perform best on *existence* questions, which is consistent with intuition since existence queries are the simplest. For KLDrive-KG, *object* and *comparison* are the most challenging categories. However, once scene facts are replaced with ground-truth annotations, these two categories improve substantially, with gains of 25.81 and 28.78 points, respectively. This suggests that fine-grained semantic QA

is highly sensitive to the fidelity of entities, attributes, and relations in the scene representation, and that improving perception quality remains critical for further end-to-end gains. In contrast, *counting* shows a relatively smaller improvement and remains one of the most difficult tasks even under ground-truth scene facts, suggesting that its difficulty lies more in the execution of complex reasoning than merely in the quality of basic scene facts.

**Objects and Attributes.** We further analyze the KLDrive-KG results from the perspectives of object categories and attributes, as shown in Figures 7. Overall, attribute-related questions are more accurate and more stable than object-related ones: the weighted accuracy is 61.50% for attribute reasoning, compared with 55.29% for object reasoning. Moreover, the variation across attributes is relatively small, whereas object-related performance differs much more substantially across categories. Specifically, objects with more distinctive visual characteristics and clearer category boundaries, such as traffic cones and bicycles, are easier to recognize, and the corresponding QA accuracy is also higher; in particular, traffic-cone-related questions are nearly saturated at 99.6%. In contrast, categories with more similar appearance and semantics, such as trucks and buses, remain considerably more challenging and yield lower QA accuracy.

**Difficulty Levels.** Next, we analyze the performance of KLDrive under different reasoning difficulty levels. To exclude the effect of perception noise, we study the results of KLDrive-GT, as shown in Figure 8. Here, *H0* (*zero-hop*) denotes factual queries that can be answered directly from the attributes of a single object, e.g., “Is there a truck in the scene?”, whereas *H1* (*one-hop*) denotes compositional queries that require relational or spatial reasoning across multiple entities, e.g., comparing the status of two vehicles at different locations. The results show that *H0* achieves consistently

high performance across all categories, while H1 is substantially more challenging. This gap is especially pronounced for *counting*, where the accuracy drops from 85.10 (H0) to 54.46 (H1). These findings indicate that once scene facts are accurately established, the remaining reasoning bottleneck mainly lies in multi-entity compositional reasoning, particularly multi-object counting and reasoning under complex spatial relations.

	Exist	Count	Object	Status	Comparison	Overall Acc
w/o KG Generation Module	53.39	12.5	16.54	8.47	48.85	28.10
w/ KG Module (KLDive-KG)	74.67	64.46	54.30	57.84	53.23	65.04
w/o LLM Agent Module	59.54	20.71	71.14	62.31	55.52	53.50
w/ LLM Agent Module (KLDive-GT)	85.55	78.92	80.11	85.72	82.01	84.49

**Table 3: Ablation comparison (accuracy%) of each functional module in KLDive illustrating the impact of KG generation model and designed LLM agent.**

### 7.3 Ablation Study

To quantify the contribution of each component in KLDive, we perform ablation study on the KG Generation model and the designed LLM agent, as summarized in Table 3.

**Perception Model.** We first validate the necessity and effectiveness of multi-source evidence aggregation and EBM-based evidence refinement. For fine-grained and complex reasoning in 3D scenes, relying on a single-modality detector is insufficient to provide a sufficiently complete fact space. To quantify this, we match detector outputs from different modalities with ground-truth objects and compute the *coverage rate*, defined as the fraction of ground-truth objects covered by at least one detection. As shown in Figure 9, the coverage rates of the camera-only (RayDN [15]) and LiDAR-only (FocalFormer3D [4]) detectors are only 40.98% and 40.18%, respectively, while the camera-LiDAR fusion detector IS-Fusion [41] increases the coverage to 77.01%. On top of this, by further aggregating multi-source detection evidence, we improve the coverage rate to 88.19%.

However, higher coverage alone is still insufficient for reliable reasoning, because the fused candidates still contain substantial noise, duplicates, and attribute conflicts. To address this, we further introduce EBM-based evidence refinement, which performs consistency modeling and global selection over multi-source candidates. As shown in Figure 10, compared with directly using the raw fused candidates, KLDive significantly improves the precision, recall, and F1-score of detected objects. This shows that EBM refinement can not only effectively recover missed objects, but also mitigate conflicts among multi-source candidates, thereby producing a more reliable structured scene representation for downstream reasoning.

We then study the gain brought by the EBM-based KG construction method. If we directly aggregate the outputs

of multi-source detectors to construct a KG and perform reasoning, the overall accuracy is only 28.10%. In contrast, KLDive-KG leverages temporal association and interpolation to recover missing objects, and uses energy-based evidence refinement to select more consistent and reliable entities and attributes from multi-source candidates, improving the overall accuracy to 65.04%, a gain of 36.94 points. This improvement is particularly evident on several key categories, including *counting*, *object*, and *status*. Overall, the ablation results show that raw detection outputs alone are insufficient to support reliable reasoning. Through EBM-based evidence refinement and structured KG construction, KLDive can more effectively recover missed objects, alleviate attribute conflicts, and build a fact space that is better suited for downstream compositional reasoning.

**LLM Agent.** We further evaluate the contribution of our LLM-agent design. Specifically, we feed the constructed KG into the same Qwen3-7B backbone for end-to-end reasoning and answer generation. The overall accuracy drops to 44.38%, showing that for complex fine-grained reasoning tasks, LLMs are prone to hallucination without an explicitly defined action space and tools. This issue is most evident on *counting* and *comparison*, where the performance gaps reach 58.21 and 26.49 points, respectively, indicating that compositional reasoning such as multi-entity filtering and comparative aggregation particularly depends on explicit tool invocation and step-by-step execution.

We then compare the importance of two key components in the KLDive agent: few-shot in-context exemplars and the *Plan-Execute-Observe* loop. Removing the in-context exemplars used to guide the LLM planner to invoke tools reduces the overall accuracy from 84.49% to 71.54%. Removing the *Plan-Execute-Observe* loop further reduces it to 62.35%. This shows that the former is crucial for stably generating correct tool-call sequences, while the latter enables the model to continually correct its reasoning through intermediate observations and thus reduces error accumulation in complex compositional reasoning. Overall, these results show that the core value of the LLM agent lies in transforming fine-grained and complex QA into a constrained, executable, and verifiable reasoning process, and the performance gains are substantial.

### 7.4 Latency Analysis

We evaluate the reasoning latency of KLDive. As shown in Figure 11, the system achieves an average latency of 1.26 s per question on an NVIDIA RTX A6000. Among all categories, *Exist* is the fastest, with an average latency of only 0.71 s, whereas comprehensive sentence-level outputs are the slowest, averaging 2.95 s. This is consistent with their

task complexity: the former usually requires only direct decisions over a small number of scene facts, whereas the latter involves a longer chain of comprehensive reasoning and sentence-level answer generation. We also observe latency differences across reasoning difficulty levels, which are especially pronounced for complex *comparison* questions. This is because H1 typically involves multi-entity localization, spatial relation resolution, and multiple tool calls, resulting in longer execution chains and higher reasoning overhead. Overall, these results show that the latency of KLDrive scales naturally with question complexity, but remains acceptable in exchange for a transparent, traceable, and verifiable reasoning process.

We further evaluate the system on an edge device, NVIDIA Jetson Orin, where the average latency is 57.05 s and follows the same trend as on the A6000. KLDrive is designed for offline fine-grained reasoning over complex driving scenes, rather than for online planning tasks with strict real-time response requirements. Therefore, considering the highly limited compute capability of Jetson and the complexity of the reasoning task, this latency is acceptable. The result indicates that KLDrive can be deployed on resource-constrained edge platforms. In future work, we will further explore lighter LLM backbones, model quantization, and reasoning-chain compression to further reduce latency and resource overhead in edge deployment.

## 8 Related Work

### 8.1 3D Scene Understanding

3D scene understanding in autonomous driving has been extensively studied along three lines: vision-based BEV methods, LiDAR-based detectors, and multi-modal fusion. Vision-based pipelines construct BEV features from multi-view images and perform 3D detection in BEV space [7, 12, 13, 15]. LiDAR-based approaches exploit sparse geometric encodings and center-based paradigms for robust long-range detection [3, 42, 48]. Fusion frameworks combine camera and LiDAR streams through BEV alignment or instance-level interaction to improve accuracy [4, 8, 14, 41]. These methods constitute the current SOTA in 3D scene perception, but they are optimized for detection metrics and produce only bounding boxes, without explicitly encoding higher-order spatial relations and supporting fine-grained factual reasoning about the scene. In this work, KLDrive transforms perception outputs into a scene knowledge graph that explicitly captures object states and spatial relations for fine-grained factual reasoning.

### 8.2 VLM & Agent for Autonomous Driving

Recent work adapts large VLMs to driving, aiming to unify perception, prediction, and planning in a language interface.

DriveGPT4 [38] and DriveVLM [31] jointly model videos and other modalities with natural-language explanations or low-level control commands; GPT-Driver[20] and LMDrive[26] use LLMs as decision modules, conditioned on multimodal perception features from cameras and LiDAR. To better structure multi-step driving decisions, Agent-Driver [21] further treats an LLM as a driving agent, combining tool use to execute the planning workflow. Domain-specific frameworks such as DriveLM, LiDAR-LLM, MAPLM, and CREMA build on general-purpose VLM backbones, attach task-specific encoders for images and point clouds, and fine-tune on large autonomous-driving data to perform language-driven perception and reasoning [2, 28, 39, 43]. These systems represent the current LLM-based SOTA on driving benchmarks, but they map sensor features to textual outputs in an end-to-end manner, making their reasoning opaque and tightly coupled to large-scale task-specific training. Our empirical study further shows that these models still hallucinate heavily on fine-grained factual queries, particularly for counting and spatial relations. In contrast, KLDrive uses a frozen 7B LLM as a tool-using planner over a structured 3D scene KG, deriving answers via explicit tool execution on the KG rather than unconstrained text generation, which reduces hallucinations significantly and obviates additional task-specific finetuning.

### 8.3 KG-Augmented LLM Reasoning

Recent work shows that augmenting LLMs with KG can reduce hallucination and improve traceability [1, 19, 23, 29, 40]. GraphRAG [6] and SubgraphRAG [10] construct or retrieve subgraphs as structured evidence for long-document and multi-hop textual QA. KERP [17], GLAME [45], and related methods [5] inject KG paths or embeddings into LLMs to guide factual reasoning and constrain model editing, while *Think-on-Graph* [29] and KG-CoT [47] explicitly treat LLMs as graph search agents that generate reasoning chains over KG to obtain interpretable answers. These studies demonstrate that combining structured KG with tool or chain-based reasoning can mitigate hallucinations. However, they are primarily developed for static symbolic knowledge graphs derived from text or curated knowledge bases, and do not address reasoning over noisy, multi-sensor, spatio-temporal 3D scenes with ego-centric geometry as required in autonomous driving. KLDrive extends KG-augmented LLM reasoning to this setting by constructing a 3D scene KG from multi-frame camera and LiDAR data, equipping it with ego-centric geometric and schema-constrained scene tools, and orchestrating them with an LLM agent to perform fine-grained, fact-grounded reasoning about autonomous-driving scenes.

## 9 Conclusion

In this paper, we study fine-grained factual reasoning in autonomous driving. We present KLDive, the first KG-based LLM reasoning framework for fine-grained question answering over 3D driving scenes. By coupling reliable scene fact construction with an LLM agent that performs explicit reasoning, KLDive produces answers grounded in verifiable scene facts rather than end-to-end black-box generation. Experiments on two large-scale autonomous-driving QA benchmarks show that KLDive consistently outperforms prior perception and LLM-based methods, while substantially reducing hallucinations on challenging fine-grained reasoning tasks. Overall, our results suggest that combining reliable scene fact construction with fact-grounded reasoning is a promising direction for more trustworthy autonomous-driving systems.

## Acknowledgements

This work has been funded in part by NSF, with award numbers #2112665, #2112167, #2003279, #2120019, #2211386, #2052809, #1911095 and in part by PRISM and CoCoSys, centers in JUMP 2.0, an SRC program sponsored by DARPA.

## References

- [1] Garima Agrawal, Tharindu Kumarage, Zeyad Alghamdi, and Huan Liu. 2024. Can knowledge graphs reduce hallucinations in llms?: A survey. In *Proceedings of the 2024 Conference of the North American Chapter of the Association for Computational Linguistics: Human Language Technologies (Volume 1: Long Papers)*. 3947–3960.
- [2] Xu Cao, Tong Zhou, Yunsheng Ma, Wenqian Ye, Can Cui, Kun Tang, Zhipeng Cao, Kaizhao Liang, Ziran Wang, James M Rehg, et al. 2024. Maplm: A real-world large-scale vision-language benchmark for map and traffic scene understanding. In *Proceedings of the IEEE/CVF conference on computer vision and pattern recognition*. 21819–21830.
- [3] Yujeong Chae, Hyeonseong Kim, Changgyoon Oh, Minseok Kim, and Kuk-Jin Yoon. 2024. Lidar-based all-weather 3d object detection via prompting and distilling 4d radar. In *European Conference on Computer Vision*. Springer, 368–385.
- [4] Yilun Chen, Zhiding Yu, Yukang Chen, Shiyi Lan, Anima Anandkumar, Jiaya Jia, and Jose M Alvarez. 2023. Focalformer3d: focusing on hard instance for 3d object detection. In *Proceedings of the IEEE/CVF international conference on computer vision*. 8394–8405.
- [5] Erica Coppelillo. 2025. Injecting Knowledge Graphs into Large Language Models. *arXiv preprint arXiv:2505.07554* (2025).
- [6] Darren Edge, Ha Trinh, Steven Truitt, and Jonathan Larson. [n. d.]. *GraphRAG: New tool for complex data discovery now on GitHub*. Microsoft Research. <https://www.microsoft.com/en-us/research/blog/graphrag-new-tool-for-complex-data-discovery-now-on-github/>
- [7] Junjie Huang, Guan Huang, Zheng Zhu, Yun Ye, and Dalong Du. 2021. Bevdet: High-performance multi-camera 3d object detection in bird-eye-view. *arXiv preprint arXiv:2112.11790* (2021).
- [8] Yang Jiao, Zequn Jie, Shaoxiang Chen, Jingjing Chen, Lin Ma, and Yu-Gang Jiang. 2023. Msmdfusion: Fusing lidar and camera at multiple scales with multi-depth seeds for 3d object detection. In *Proceedings of the IEEE/CVF conference on computer vision and pattern recognition*. 21643–21652.
- [9] Yann LeCun, Sumit Chopra, Raia Hadsell, M Ranzato, Fugie Huang, et al. 2006. A tutorial on energy-based learning. *Predicting structured data 1*, 0 (2006).
- [10] Mufei Li, Siqi Miao, and Pan Li. 2024. Simple is effective: The roles of graphs and large language models in knowledge-graph-based retrieval-augmented generation. *arXiv preprint arXiv:2410.20724* (2024).
- [11] Yue Li, Meng Tian, Zhenyu Lin, Jiangtong Zhu, Dechang Zhu, Haiqiang Liu, Yueyi Zhang, Zhiwei Xiong, and Xinhai Zhao. 2025. Fine-grained evaluation of large vision-language models in autonomous driving. In *Proceedings of the IEEE/CVF International Conference on Computer Vision*. 9431–9442.
- [12] Zhenxin Li, Shiyi Lan, Jose M Alvarez, and Zuxuan Wu. 2024. Bevnex: Reviving dense bev frameworks for 3d object detection. In *Proceedings of the IEEE/CVF conference on computer vision and pattern recognition*. 20113–20123.
- [13] Zhiqi Li, Wenhai Wang, Hongyang Li, Enze Xie, Chonghao Sima, Tong Lu, Qiao Yu, and Jifeng Dai. 2022. Bevformer: Learning bird’s-eye-view representation from multi-camera images via spatiotemporal transformers.(2022). URL <https://arxiv.org/abs/2203.17270> (2022).
- [14] Tingting Liang, Hongwei Xie, Kaicheng Yu, Zhongyu Xia, Zhiwei Lin, Yongtao Wang, Tao Tang, Bing Wang, and Zhi Tang. 2022. Bevfusion: A simple and robust lidar-camera fusion framework. *Advances in Neural Information Processing Systems* 35 (2022), 10421–10434.
- [15] Feng Liu, Tengeng Huang, Qianjing Zhang, Haotian Yao, Chi Zhang, Fang Wan, Qixiang Ye, and Yanzhao Zhou. 2024. Ray denoising: Depth-aware hard negative sampling for multi-view 3d object detection. In *European Conference on Computer Vision*. Springer, 200–217.
- [16] Haotian Liu, Chunyuan Li, Yuheng Li, and Yong Jae Lee. 2024. Improved Baselines with Visual Instruction Tuning. In *Proceedings of the IEEE/CVF Conference on Computer Vision and Pattern Recognition (CVPR)*. 26296–26306.
- [17] Haochen Liu, Song Wang, Yaochen Zhu, Yushun Dong, and Jundong Li. 2024. Knowledge graph-enhanced large language models via path selection. *arXiv preprint arXiv:2406.13862* (2024).
- [18] Hanchao Liu, Wenyuan Xue, Yifei Chen, Dapeng Chen, Xiutian Zhao, Ke Wang, Liping Hou, Rongjun Li, and Wei Peng. 2024. A survey on hallucination in large vision-language models. *arXiv preprint arXiv:2402.00253* (2024).
- [19] Chuangtao Ma, Sriom Chakrabarti, Arijit Khan, and Bálint Molnár. 2025. Knowledge graph-based retrieval-augmented generation for schema matching. *arXiv preprint arXiv:2501.08686* (2025).
- [20] Jiageng Mao, Yuxi Qian, Junjie Ye, Hang Zhao, and Yue Wang. 2023. Gpt-driver: Learning to drive with gpt. *arXiv preprint arXiv:2310.01415* (2023).
- [21] Jiageng Mao, Junjie Ye, Yuxi Qian, Marco Pavone, and Yue Wang. 2023. A language agent for autonomous driving. *arXiv preprint arXiv:2311.10813* (2023).
- [22] Ana-Maria Marcu, Long Chen, Jan Hünemann, Alice Karnsund, Benoit Hanotte, Prajwal Chidananda, Saurabh Nair, Vijay Badrinarayanan, Alex Kendall, Jamie Shotton, et al. 2024. Lingoqa: Visual question answering for autonomous driving. In *European Conference on Computer Vision*. Springer, 252–269.
- [23] Nur A Zarin Nishat, Andrea Coletta, Luigi Bellomarin, Kossi Amouzouvi, Jens Lehmann, and Sahar Vahdati. 2025. Aligning Knowledge Graphs and Language Models for Factual Accuracy. *arXiv preprint arXiv:2507.13411* (2025).
- [24] Shuai Peng, Di Fu, Liangcai Gao, Xiuqin Zhong, Hongguang Fu, and Zhi Tang. 2024. Multimath: Bridging visual and mathematical reasoning for large language models. *arXiv preprint arXiv:2409.00147* (2024).
- [25] Tianwen Qian, Jingjing Chen, Linhai Zhuo, Yang Jiao, and Yu-Gang Jiang. 2024. Nuscenes-qa: A multi-modal visual question answering

- benchmark for autonomous driving scenario. In *Proceedings of the AAAI Conference on Artificial Intelligence*, Vol. 38. 4542–4550.
- [26] Hao Shao, Yuxuan Hu, Letian Wang, Guanglu Song, Steven L Waslander, Yu Liu, and Hongsheng Li. 2024. Lmdrive: Closed-loop end-to-end driving with large language models. In *Proceedings of the IEEE/CVF Conference on Computer Vision and Pattern Recognition*. 15120–15130.
- [27] Jianxin Shi, Jinhao Chen, Yuandong Wang, Li Sun, Chunyang Liu, Wei Xiong, and Tianyu Wo. 2025. Motion forecasting for autonomous vehicles: a survey. *arXiv preprint arXiv:2502.08664* (2025).
- [28] Chonghao Sima, Katrin Renz, Kashyap Chitta, Li Chen, Hanxue Zhang, Chengen Xie, Jens Beißwenger, Ping Luo, Andreas Geiger, and Hongyang Li. 2024. Drivelm: Driving with graph visual question answering. In *European conference on computer vision*. Springer, 256–274.
- [29] Jiashuo Sun, Chengjin Xu, Lumingyuan Tang, Saizhuo Wang, Chen Lin, Yeyun Gong, Lionel M Ni, Heung-Yeung Shum, and Jian Guo. 2023. Think-on-graph: Deep and responsible reasoning of large language model on knowledge graph. *arXiv preprint arXiv:2307.07697* (2023).
- [30] Qwen Team. 2025. Qwen3 Technical Report. arXiv:2505.09388 [cs.CL] <https://arxiv.org/abs/2505.09388>
- [31] Xiaoyu Tian, Junru Gu, Bailin Li, Yicheng Liu, Yang Wang, Zhiyong Zhao, Kun Zhan, Peng Jia, Xianpeng Lang, and Hang Zhao. 2024. Drivevlm: The convergence of autonomous driving and large vision-language models. *arXiv preprint arXiv:2402.12289* (2024).
- [32] Ke Wang, Junting Pan, Weikang Shi, Zimu Lu, Houxing Ren, Aojun Zhou, Mingjie Zhan, and Hongsheng Li. 2024. Measuring multimodal mathematical reasoning with math-vision dataset. *Advances in Neural Information Processing Systems* 37 (2024), 95095–95169.
- [33] Weiyun Wang, Zhangwei Gao, Lixin Gu, Hengjun Pu, Long Cui, Xingguang Wei, Zhaoyang Liu, Linglin Jing, Shenglong Ye, Jie Shao, et al. 2025. InternVL3.5: Advancing Open-Source Multimodal Models in Versatility, Reasoning, and Efficiency. *arXiv preprint arXiv:2508.18265* (2025).
- [34] Xintong Wang, Jingheng Pan, Liang Ding, and Chris Biemann. 2024. Mitigating hallucinations in large vision-language models with instruction contrastive decoding. *arXiv preprint arXiv:2403.18715* (2024).
- [35] Taokai Xia and Hui Chen. 2024. A survey of autonomous vehicle behaviors: Trajectory planning algorithms, sensed collision risks, and user expectations. *Sensors* 24, 15 (2024), 4808.
- [36] Xinyue Xu, Yi Qin, Lu Mi, Hao Wang, and Xiaomeng Li. 2024. Energy-based concept bottleneck models: Unifying prediction, concept intervention, and probabilistic interpretations. *arXiv preprint arXiv:2401.14142* (2024).
- [37] Zelai Xu, Zhexuan Xu, Xiangmin Yi, Huining Yuan, Xinlei Chen, Yi Wu, Chao Yu, and Yu Wang. 2025. VS-Bench: Evaluating VLMs for Strategic Reasoning and Decision-Making in Multi-Agent Environments. *arXiv preprint arXiv:2506.02387* (2025).
- [38] Zhenhua Xu, Yujia Zhang, Enze Xie, Zhen Zhao, Yong Guo, Kwan-Yee K Wong, Zhenguo Li, and Hengshuang Zhao. 2024. Drivegpt4: Interpretable end-to-end autonomous driving via large language model. *IEEE Robotics and Automation Letters* (2024).
- [39] Senqiao Yang, Jiaming Liu, Renrui Zhang, Mingjie Pan, Ziyu Guo, Xiaoqi Li, Zehui Chen, Peng Gao, Hongsheng Li, Yandong Guo, et al. 2025. Lidar-llm: Exploring the potential of large language models for 3d lidar understanding. In *Proceedings of the AAAI Conference on Artificial Intelligence*, Vol. 39. 9247–9255.
- [40] Weiqi Ye, Qiang Zhang, Xian Zhou, Wenpeng Hu, Changhai Tian, and Jiajun Cheng. 2024. Correcting Factual Errors in LLMs via Inference Paths Based on Knowledge Graph. In *2024 International Conference on Computational Linguistics and Natural Language Processing (CLNLP)*. IEEE, 12–16.
- [41] Junbo Yin, Jianbing Shen, Runnan Chen, Wei Li, Ruigang Yang, Pascal Frossard, and Wenguan Wang. 2024. Is-fusion: Instance-scene collaborative fusion for multimodal 3d object detection. In *Proceedings of the IEEE/CVF conference on computer vision and pattern recognition*. 14905–14915.
- [42] Tianwei Yin, Xingyi Zhou, and Philipp Krahenbuhl. 2021. Center-based 3d object detection and tracking. In *Proceedings of the IEEE/CVF conference on computer vision and pattern recognition*. 11784–11793.
- [43] S Yu, J Yoon, and M Bansal. 2025. CREMA: Generalizable and Efficient Video-language Reasoning via Multimodal Modular Fusion. *Proceedings of the International Conference on Learning Representations*.
- [44] Zhou Yu, Jun Yu, Yuhao Cui, Dacheng Tao, and Qi Tian. 2019. Deep modular co-attention networks for visual question answering. In *Proceedings of the IEEE/CVF conference on computer vision and pattern recognition*. 6281–6290.
- [45] Mengqi Zhang, Xiaotian Ye, Qiang Liu, Pengjie Ren, Shu Wu, and Zhumin Chen. 2024. Knowledge graph enhanced large language model editing. *arXiv preprint arXiv:2402.13593* (2024).
- [46] Jingyuan Zhao, Yuyan Wu, Rui Deng, Susu Xu, Jinpeng Gao, and Andrew Burke. 2025. A survey of autonomous driving from a deep learning perspective. *Comput. Surveys* 57, 10 (2025), 1–60.
- [47] Ruilin Zhao, Feng Zhao, Long Wang, Xianzhi Wang, and Guandong Xu. 2024. Kg-cot: Chain-of-thought prompting of large language models over knowledge graphs for knowledge-aware question answering. In *Proceedings of the Thirty-Third International Joint Conference on Artificial Intelligence (IJCAI-24)*. International Joint Conferences on Artificial Intelligence, 6642–6650.
- [48] Zixiang Zhou, Xiangchen Zhao, Yu Wang, Panqu Wang, and Hassan Foroosh. 2022. Centerformer: Center-based transformer for 3d object detection. In *European Conference on Computer Vision*. Springer, 496–513.